Chemical Engineering Science 69 (2012) 373–381

Contents lists available at SciVerse ScienceDirect

Chemical Engineering Science

journal homepage: www.elsevier.com/locate/ces

The measurement of powder flow properties with a mechanically stirred aerated bed

Igino Tomasetta [a], Diego Barletta [a], Paola Lettieri [b], Massimo Poletto [a,*]

[a] Dipartimento di Ingegneria Industriale, Università degli Studi di Salerno, Via Ponte Don Melillo, 84084 Fisciano, SA, Italy
[b] Department of Chemical Engineering, University College London, Torrington Place, London WC1E 7JE, UK

ARTICLE INFO

Article history:
Received 29 July 2010
Received in revised form
6 August 2011
Accepted 25 October 2011
Available online 6 November 2011

Keywords:
Powder flow properties
Aerated powders
Powder technology
Solid mechanics
Rheology
Fluidization

ABSTRACT

This paper re-examines a set of experimental data published by Bruni et al. (2007a, 2007b) [Bruni, G., Barletta, D., Poletto, M., Lettieri, P., 2007a. A rheological model for the flowability of aerated fine powders. Chem. Eng. Sci. 62, 397–407; Bruni, G., Lettieri, P., Newton, D., Barletta, D., 2007b. An investigation of the effect of the interparticle forces on the fluidization behaviour of fine powders linked with rheological studies. Chem. Eng. Sci. 62, 387–396] carried out on a mechanically stirred fluid-bed rheometer (msFBR), which was developed to study the rheology of aerated and fluidized powders. The use of aeration below fluidization allowed to carry out experiments with powders at very low consolidation levels. Two mathematical models, based on the Janssen approach to evaluate stresses in powder containers, were developed in order to relate the torque measurements in the Fluidized Bed Rheometer to the flow properties of the powders measured with standard powder flow testers. Results indicate that the models were able to satisfactorily predict the torque measured by the msFBR. The larger complexity of the Walker (1966) [Walker, D.M., 1966. An approximate theory for pressures and arching in hoppers, Chem. Eng. Sci. 21, 975–997] and Walters (1973) [Walters, J.K., 1973. A theoretical analysis of stresses in silos with vertical walls, Chem. Eng. Sci. 28, 13–21] stress analysis adopted in one of the two models did not introduce significant improvements in the evaluation of the stress distribution to justify its use. A procedure for the inverse application of the model was developed and applied to estimate the powder flow properties starting from msFBR data. The application of this procedure provided good results in terms of effective angle of internal friction and is promising for the ability of the system to explore powder flow at very low consolidation states.

© 2011 Elsevier Ltd. All rights reserved.

1. Introduction

The flow properties of fine powders at very low consolidation levels are relevant to small scale industrial application of powder flow, such as in small process hoppers and mixers of pharmaceutical powders (Harnby, 2000), or in everyday applications such as toner flow in cartridges (Suri and Horio, 2009) and dosing and dispersion in dry powder inhalers (Daniher and Zhu, 2008).

Conventional shear testers are not suitable for testing flow properties of loosely consolidated powders unless special procedures are adopted (Schwedes, 2003). In particular, consolidation stresses lower than 500 Pa were obtained in annular shear cells by applying small normal loads and increasing the sensitivity of load cells (Schulze and Wittmaier, 2003) or by introducing a gas pressure gradient opposed to gravity through the powder sample (Klein et al., 2003; Johanson and Barletta, 2004; Barletta et al., 2007). Alternative techniques used to study the rheological properties of powders under loose conditions included the derivation of the tensile strength and of yield loci from fluidization experiments (Castellanos et al., 2004) and the derivation of cohesion and angle of friction from observations of the avalanching behavior of powders (Castellanos et al., 2007). Studies on the rheological behavior of slow dense powder flows were performed also by rotational rheometers of different geometries. In particular, Tardos and co-workers (Tardos et al., 1998, 2003; Kheiripour Langroudi et al., 2010) measured local normal stresses and the overall torque necessary to shear powders in a Couette device at different consolidation stresses obtained by varying the powder bed depth. Measurement results indicated that solid normal stresses show a linear hydrostatic profile from the bed free surface to the bed bottom while shearing both a low and at intermediate shear rates (dimensionless shear rates, defined as $\dot{\gamma}^* = \dot{\gamma}(d_p/g)^{0.5}$, between 0.1 and 1). These results differ from the experimental evidence that in static powder beds the solid normal stresses increase less than linearly up to an asymptotic value as predicted by the Janssen equation. Nevertheless, torque measurements confirmed a frictional behavior of powders at low shear rates and a "viscous" behavior at intermediate shear rates for which Tardos et al. (2003) and Kheiripour Langroudi et al. (2010) proposed

* Corresponding author. Tel.: +39 89964132; fax: +39 89964057.
E-mail address: mpoletto@unisa.it (M. Poletto).

0009-2509/$ - see front matter © 2011 Elsevier Ltd. All rights reserved.
doi:10.1016/j.ces.2011.10.056

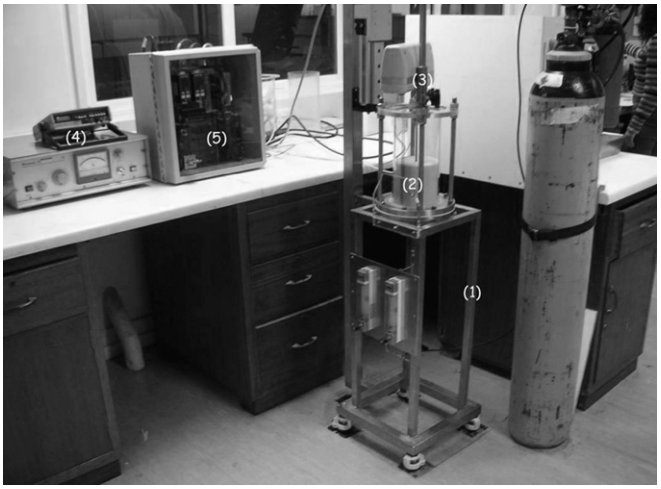

Fig. 1. The msFBR unit. It was mounted on a free standing, wheeled stainless steel frame (1), and consists of a fluidization unit (2), an agitating system (3), a data acquisition unit (4) and a control box (5).

a constitutive equation following a continuum mechanics approach. A mechanically stirred fluid-bed rheometer (msFBR) (Fig. 1) was developed by Bruni et al. (2005) to study the rheology of aerated and fluidized powders. This device, consisting in a fluidized bed column provided with a two-flat-bladed paddle impeller immersed in the powder bed and connected to a rheometer, was used for powders under aerated conditions below the fluidization threshold, allowing to measure powder flow properties at very low consolidation levels. In fact, the upwards gas flow produces a vertical gas pressure gradient, which acts on the solids as a body force opposed to gravity. The torque necessary to rotate the impeller was measured at different powder bed depths and gas pressure drops. Results obtained at very low shear rates (0.754 rpm, corresponding to a dimensionless shear rate between 3.5×10^{-5} and 7.5×10^{-5} depending on the particle size) revealed that torque vertical profiles followed the Janssen equation. Consequently, Bruni et al. (2007a) developed a model based on the method of differential slices (Janssen's approach) and on a Mohr–Coulomb description of the powder rheology to describe the powder stress state and the applied torque in the msFBR.

In the present study, the introduction of the Walker improvements (Walker, 1966; Walters, 1973) for the stress state in the model developed by Bruni et al. (2007a) following the Janssen approach was assessed. Moreover, a sensitivity analysis is performed in order to estimate the relative weight of the angle of wall friction on the prediction of torques. Finally, an inverse procedure to evaluate powder flow properties from torques is proposed.

2. The model

In order to predict the torques measured by the msFBR, a rheological model had been developed by Bruni et al. (2007a). To determine the stress distribution in the msFBR the original Janssen analysis for silo stress distribution had been generalized taking into account the air flow through the bed. According to this analysis, stresses had been assumed uniform across any horizontal section of the material. Furthermore, the axial and radial stresses, σ_z and σ_r, had been assumed as principal stresses.

The stress state in the msFBR had been evaluated solving the balance force on a differential slice of the cylindrical vessel as sketched in Fig. 2, which gives the following differential equation:

$$\frac{d\sigma_z}{dz}+\frac{4\tau_W}{D}=\rho_b g-\frac{dP}{dz} \tag{1}$$

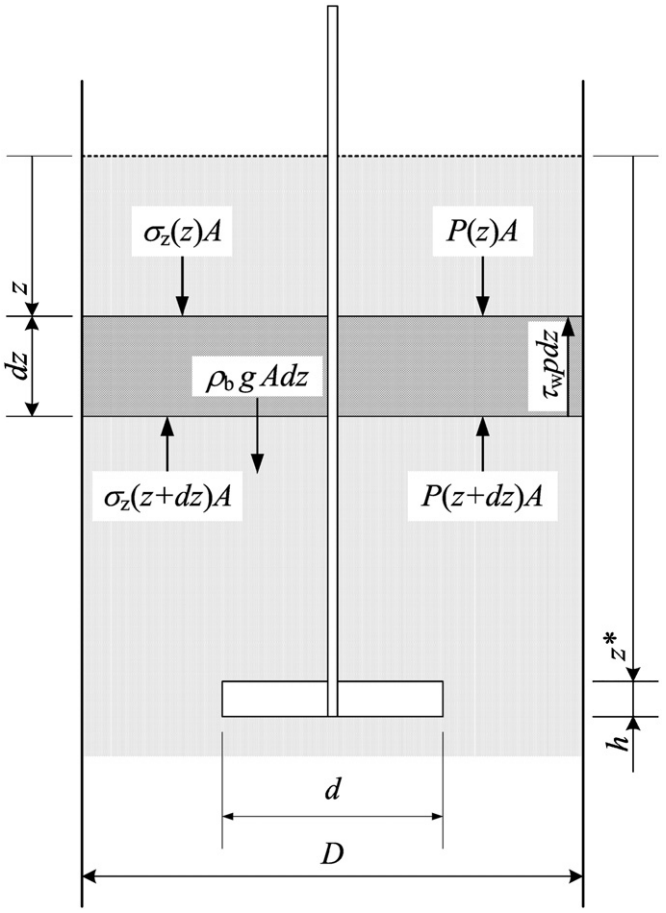

Fig. 2. Scheme of the msFBR with the most significant variables used in the models.

where τ_W is the shear stress acting on the wall, ρ_b is the bulk density of the powder and dP/dz is the pressure gradient of the air flowing through the bed and exerting a drag force opposed to the gravity. In order to solve this equation, a relationship between the wall shear stress τ_W and the vertical normal stress σ_z had been necessary, since ρ_b and dP/dz had been measured in each experiment and considered constant along all the bed. Following Janssen (1895), the wall yield locus and the ratio of the axial and radial stresses, K, had been introduced as the two relationships, which had allowed to solve the problem

$$\tau_W=\sigma_r(z)\tan\phi_W \tag{2}$$

$$K=\frac{\sigma_r}{\sigma_z} \tag{3}$$

where ϕ_W is the angle of wall friction.

Finally, the top surface of the bed of material had been assumed open to the atmosphere so that

$$\sigma_z(z=0)=0 \tag{4}$$

To evaluate the torque acting on the impeller in the msFBR, the shearing surface around the impeller had been assumed to be shaped like the flat cylinder described by the impeller rotation, having height h and diameter d equal to the height of the impeller paddle and to the double of the distance between the paddle tip and the shaft axis. It is assumed that the largest shearing action produced by the impeller is likely to be close to the impeller itself.

The resistant torque will be the sum of the contributions of the stresses acting on the upper surface, the lower surface and the

lateral surface:

$$T = T_{up} + T_{down} + T_{lateral} \quad (5)$$

Due to the small impeller height, the stress variations in the region around the impeller had been neglected. Thus, the stresses around the impeller had been equated to the stresses at a depth z^* immediately above the impeller (Fig. 2). Therefore,

$$T_{up} = T_{down} = \int_o^{d/2} \tau_{z\theta}(z^*) 2\pi r^2 \, dr \quad (6)$$

$$T_{lateral} = \frac{\pi}{2} d^2 \int_{z^*}^{z^*+h} \tau_{r\theta}(z) dz = \frac{\pi}{2} \tau_{r\theta}(z^*) d^2 h \quad (7)$$

In order to solve the differential equation (1), which allows to obtain the stress distribution into the msFBR and to estimate the measured torque, it is necessary to select proper relationships describing mobilization conditions of the powder.

The parameter K is an important parameter appearing in standardized silo design procedures and it should be measured directly (EN 1991-4, 2006). Presently, however, a standardized procedure to evaluate it is not yet defined. Experimental evaluations (i.e. Kwade et al., 1994) indicate that it ranges between 0.4 and 0.7. In the lack of a direct experimental evaluation of K some authors (i.e. Nedderman, 1992) assume full internal mobilization and correspondingly use the Mohr–Coulomb condition, for which the Mohr circle is tangent to the yield locus at the failure plane of the powder. In this way it is possible to obtain a relationship for K as a function of the failure properties of the experimental materials by simple geometric considerations on the Mohr–Coulomb criterion. It has to be recognized, however, that not always directly measured values of K are close to the Mohr–Coulomb estimate, suggesting that the solids do not reach a condition of full mobilization in the container.

Assuming the Mohr–Coulomb condition, the effective yield locus is commonly used to define the failure behavior of powders for granular materials with low cohesion, like the experimental materials analyzed in this work. With the effective yield locus, the equation for the K ratio will depend only on the effective angle of internal friction δ and can be written as

$$K = \frac{1 + \kappa \sin\delta}{1 - \kappa \sin\delta} \quad (8)$$

where the parameter κ takes into account the active and passive state of the powder. In particular, it is

- $\kappa = 1$ passive state ($\sigma_r > \sigma_z$, σ_r is the major principal stress);
- $\kappa = -1$ active state ($\sigma_z > \sigma_r$, σ_z is the major principal stress).

The state of stresses in the msFBR was evaluated by solving simultaneously Eqs. (1)–(3) and (8) with the boundary condition (4) for the passive and active state. Since the effective angle of internal friction is a function of the major principal stresses, in turn function of the depth of the bed, the K ratio is variable with the depth of the bed. Therefore, a numerical solution was needed.

For the estimation of the torque, the expressions of the shear stresses acting on the shearing surface are

$$\tau_{z\theta}(z^*) = \sigma_z(z^*) \tan\delta \quad (9)$$

$$\tau_{r\theta}(z^*) = \sigma_r(z^*) \tan\delta = K \sigma_z(z^*) \tan\delta \quad (10)$$

Values of the predicted torques can be obtained using (9) and (10) in Eqs. (6) and (7).

2.1. Walker's improvements

The assumptions of the previous model that the axial and radial stresses are principal stresses and uniform across any horizontal section of the bed are clearly erroneous. They are, in fact, in contrast with the presence of vertical shear stresses at the wall. In order to correct this inconsistency, Walker (1966) defined a mean axial stress as

$$\frac{\pi D^2}{4} \overline{\sigma}_z = \int \sigma_z \, dA \quad (11)$$

and rewrote the force balance on the differential slice, which then becomes

$$\frac{d\overline{\sigma}_z}{dz} + \frac{4\tau_W}{D} = \rho_b g - \frac{dP}{dz} \quad (12)$$

Similarly to previous case, to solve this differential equation, we need some functional relationships between the wall shear stress and the mean axial stress. Considering the wall yield locus we have

$$\tau_W = (\sigma_r)_W \tan\phi_W \quad (13)$$

Walker studied in greater detail the Mohr–Coulomb criterion at the wall plane. Assuming the material in incipient downward motion along the wall, Walker calculated the ratio of the radial and axial stresses in the wall region as

$$K_W = \left(\frac{\sigma_r}{\sigma_z}\right)_W = \frac{1 + \kappa \sin\delta \cos(\omega + \kappa\phi_W)}{1 - \kappa \sin\delta \cos(\omega + \kappa\phi_W)} \quad (14)$$

where

$$\sin\omega = \frac{\sin\phi_W}{\sin\delta} \quad (15)$$

and κ is the parameter, which takes into account the active and the passive state. In order to solve the differential equation (12), Walker defined a distribution factor $\mathcal{D}$ as the ratio of the axial stress at the wall and the mean axial stress. On the Walker assumption that the radial normal stress σ_r is constant over the cross section, $\sigma_r = (\sigma_r)_W$, Walters (1973) calculated the distribution factor at great depths as

$$\mathcal{D} = \frac{(\sigma_z)_W}{\overline{\sigma}_z} = \frac{1 - \sin^2\delta - 2\kappa \sin\delta \sqrt{(1-c)}}{1 + \sin^2\delta - (4/3c)\kappa \sin\delta [1 - (1-c)^{3/2}]} \quad (16)$$

where

$$c = \tan^2\phi_W / \tan^2\delta \quad (17)$$

Assuming Eq. (16) for $\mathcal{D}$ along all the bed height and solving simultaneously Eqs. (12)–(17) with the boundary condition

$$\overline{\sigma}_z(z = 0) = 0 \quad (18)$$

it is possible to obtain the distribution of the mean axial normal stress with the depth in the msFBR.

To predict the contributions of the torque on the upper and lower surfaces by Eq. (6), an analytical relationship is necessary for the axial normal stress σ_z as a function of the radius r of the bed. According to the Walters analysis, it is

$$\sigma_z(r,z) = \sigma_r(z) \frac{1 + \sin^2\delta - 2\kappa \sin\delta \sqrt{1 - c(2r/D)^2}}{\cos^2\delta} \quad (19)$$

With these hypotheses, the shear stresses acting on the shearing surface can be written as

$$\tau_{z\theta}(r,z^*) = \sigma_z(r,z^*) \tan\delta = K_W \mathcal{D} \overline{\sigma}_z(z^*) \frac{1 + \sin^2\delta - 2\kappa \sin\delta \sqrt{1 - c(2r/D)^2}}{\cos^2\delta} \tan\delta \quad (20)$$

$$\tau_{r\theta}\left(\frac{d}{2}, z^*\right) = \sigma_r\left(\frac{d}{2}, z^*\right) \tan\delta = (\sigma_r)_W(z^*) \tan\delta = K_W \mathcal{D} \overline{\sigma}_z(z^*) \tan\delta \quad (21)$$

At this point, the contributions of the predicted torque on the upper, lower and lateral surfaces can be calculated by solving the integrals in (6) and (7) by the use of Eqs. (20) and (21).

3. Experimental

3.1. Apparatus

The torque necessary to rotate an impeller in an aerated bed of powders was measured with a mechanically stirred Fluidized Bed Rheometer (msFBR), shown in Fig. 1. The msFBR was designed and built at UCL. It consists of a fluidization unit, an agitating system and a data acquisition unit. In particular, the fluidization unit is a 140 mm internal diameter × 300 mm tall Pyrex vessel fitted with a sintered stainless steel distributor plate. A 70 mm high windbox filled by 10 mm ceramic balls is located below the distributor plate in order to allow a more uniform distribution of the gas. Nitrogen was used as fluidizing gas. A steel shaft 165 mm long with a two-blades rectangular impeller (36 mm × 7 mm high and 0.7 mm thickness) is driven by a rotational rheometer form the agitating system. The braking torque and the pressure drop across the bed are measured.

Details regarding this apparatus and its use on fluidized beds are reported by Bruni et al. (2005). Experimental results obtained below the minimum fluidization condition and the effect of the impeller depth and the aeration are given by Bruni et al. (2007a).

Yield loci of three different samples of alumina powder and glass ballotini were measured by a Schulze shear tester (Ring Shear Tester 01.01). It consists of an annular bottom ring filled by powder and a lid. For a specified normal load, the torque required to the rotation of the lid is measured. The standard procedure consists of two steps: *preshear*, under normal stress up to a steady shear stress, and subsequent *shear*, under a normal stress lower than the *preshear stress* up to a peak shear stress. The two steps are repeated for the same *preshear* and for decreasing *shear* normal loads. In the *shear* step, the peak values of the shear stresses and the corresponding normal stress will be the point coordinates constituting the yield locus of the powder at the specified *preshear* consolidation level.

A Jenike shear tester was used to evaluate the wall friction of the experimental materials. To this purpose, the base of the cell was replaced by a sample of Pyrex, similar to the material of the wall of the msFBR. The procedure adopted for testing the wall yield locus of experimental materials is reported on the "Standard Shear Testing Technique" (1989).

3.2. Materials

The materials used in these experiments are three alumina powders and a glass ballotini powder, whose properties are summarized in Table 1. The alumina A0 is a virtually fines free powder while Alumina A5 and A6 contain the same total amount of fines (F_x indicates the weight cumulative smaller than x) but shifted towards bigger (26–45 μm) or smaller (0–25 μm) size cuts, respectively.

Table 1
Material properties.

Materials	d_p (Sauter) (μm)	F_{25}	F_{45}	ρ_p (kg m^{-3})	ϕ_W (deg.)	ϕ_W[a] (deg.)	ϕ_W[b] (deg.)
Alumina A0	75.1	0.0	3.2	1730	22.1	12.7	13.6
Alumina A5	49.1	8.1	30.7	1730	19.7	13.8	14.9
Alumina A6	36	18.8	30.9	1730	21.1	16.8	19.4
Ballotini	350	–	–	2500	12.2	15.7	17.6

[a] Values obtained from msFBR data considering the model developed by Bruni et al. (2007a).
[b] Values obtained from msFBR data adopting the Walker improvements.

Table 2
Symbols used in Figs. 5, 6 and 8.

Symbol	○●	□■	△▲	◇◆
Materials	$\Delta P/\Delta P_c$			
Alumina A0	0.0	0.25	0.46	0.80
Alumina A5	0.0	0.33	0.69	0.94
Alumina A6	0.0	0.24	0.48	0.71
Ballotini	0.0	0.24	0.48	0.75

These materials were already analyzed by Bruni et al. (2007b) in order to evaluate the effect of interparticle forces regulated by the percentage of fines on the fluidization behavior.

4. Experimental results

4.1. Internal failure properties

The bulk powder flow properties of the three alumina sample A0, A5 and A6 and of the glass ballotini, measured by a Schulze Ring Shear Tester, were used to evaluate the effective angle of internal friction, reported by filled symbols in Fig. 3 as a function of the major principal stress. Inspection of this figure indicates that the alumina samples A0, A5 and A6 are characterized by very similar effective angles of internal friction while ballotini have significantly lower values. The difference for the internal friction is probably due to the perfectly round shape and the low rugosity of glass ballotini, which make shearing easier.

4.2. Wall friction properties

Results of the wall friction properties of the experimental materials on a sample of Pyrex, measured on the Jenike shear cell, are reported in Fig. 4. In this figure wall yield loci were evaluated by plotting the best fitting line to the experimental data points (σ, τ). All the materials were considered adhesionless with a good agreement with the experimental measurements. The values of the angle of wall friction are reported in column 6 of Table 1.

5. Results and discussion

The first step of this work was to determine the better description of experimental data between the active and the passive state of stress. Fig. 5 shows the comparisons between the values predicted with the model based on the Janssen approach (Bruni et al., 2007a), assuming passive and active state, and the experimental torque data. In particular, profiles at different levels of aeration, referred as the ratio $\Delta P/\Delta P_c$ between the measured pressure drop across the bed and the pressure drop at minimum fluidization ($\Delta P_c = Mg/A$), are reported. As above said, all the experiments were carried out below the minimum for fluidization and, therefore it is always $\Delta P/\Delta P_c < 1$. The match between predicted and experimental data is better for glass ballotini where the model slightly overestimates the measured torques. Instead, for alumina samples the match is worse, in particular for the Alumina A5 for high values of $\Delta P/\Delta P_c$ ($\Delta P/\Delta P_c = 0.94$).

Although the predicted data did not show a good agreement with the experimental data, the passive state model seems to better describe the rheological behavior in the msFBR. In fact, for all the materials and at all the aeration rates tested, the passive state allows to attain the asymptotic values of the torque at distances closer to the experiments than the active state model. It

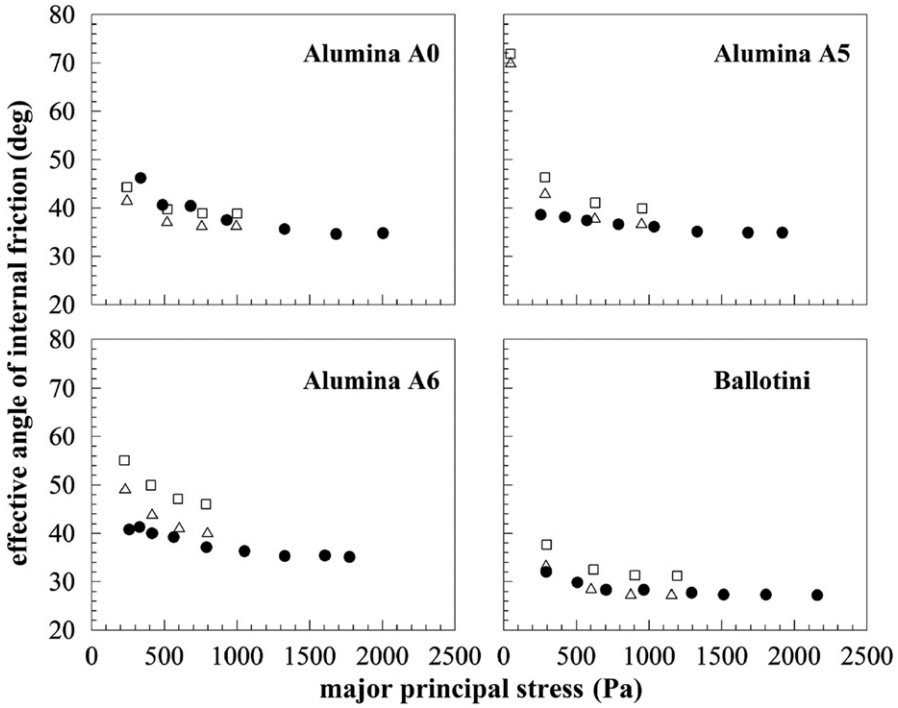

Fig. 3. Values of the effective angle of internal friction δ as a function of the major principal stress σ_1 for the different materials tested: ●, experimental data; △, estimated data by the model based on Janssen's approach; □, estimated data by the model including Walker's improvements.

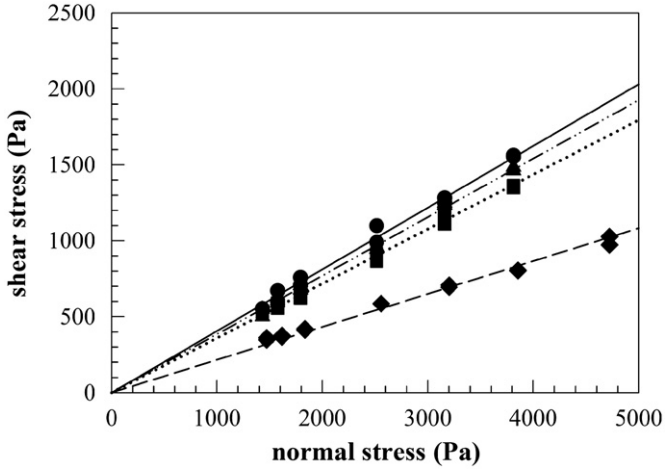

Fig. 4. Wall yield loci (τ vs. σ) for the different materials tested: ●, ————, Alumina A0; ■, - - - -, Alumina A5; ▲, —— - -, Alumina A6; ♦,— — —, Ballotini. Symbols are experimental point, lines come from linear regression.

is likely, therefore, that a passive state of stresses sets up during the experiments, probably due to the centrifugal action of the impeller, which drew material from the bed axis. In the following analysis, all the other results presented will refer to the hypothesis that a passive state was setting up within the bed.

The second step in this work was a more accurate evaluation of the stress state in the msFBR. Fig. 6 shows a comparison between experimental values and predicted results by the model based on Janssen's hypothesis and the model adopting Walker's improvements. Fig. 6 reveals that the estimated torques by the latter model are slightly lower than those obtained by the former. This can be somehow explained by observing the construction of Mohr's circles at the wall and at the center of the bed for passive state, showed in Fig. 7 according to Walters (1973). Taking into account that the axial and the radial directions are principal directions at the axis of the bed, the applied stresses on the shearing surface, developed by the rotation of paddles of the impeller around the bed axis, are therefore lower than the stresses calculated by the first model, which considers normal and radial stresses as principal and uniform over the bed cross section.

On the other hand, torques estimated by the model assuming the Walker improvements for glass ballotini show a better agreement than the first model with the experimental results.

5.1. Sensitivity analysis on wall failure properties

The wall friction measurements were made on a similar material, but not the same used for the construction of the msFBR walls. Furthermore, wall shear stress measurement may bear large differences between the measurement conditions and the process operating conditions. In fact, these differences are still a subject of scientific debate. These considerations suggest a certain care in the use of the measured valued of the wall friction angle. In order to evaluate the relevance of a correct estimation of the angle of wall friction on the torque predictions, a sensitivity analysis of the angle of wall friction was performed, considering variations of ϕ_w between $\pm 20\%$. These variations produce variations of the predicted torques between about -17% and 20% for Alumina samples and between about -10.5% and 12% for glass ballotini. The less significant changes of the predicted torques for glass ballotini are probably due to the lower relative weight of the wall friction as a consequence of the greater density of this experimental material, which implies higher stresses inside the bulk solids, and the lower value of the measured angle of wall friction. More in general, these results confirms that the uncertainty in the correct evaluation of the wall friction coefficient determine a similar uncertainty in the final model results. Therefore, the large differences between experimental and predicted torques for the Alumina powders could be attributed to an

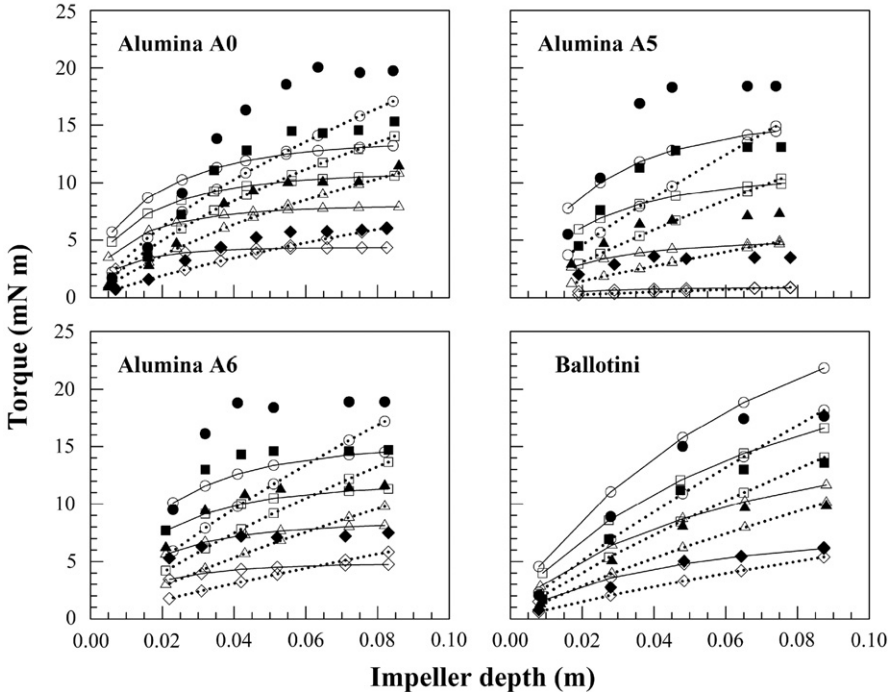

Fig. 5. Comparison between experimental and estimated torques values T vs. impeller depth z^* for different values of $\Delta P/\Delta P_c$ (symbols in Table 2). The model is based on the simple Janssen's approach. Filled symbols, experimental data. Hollow symbols and lines, predicted data: ————, passive state; - - - -, active state.

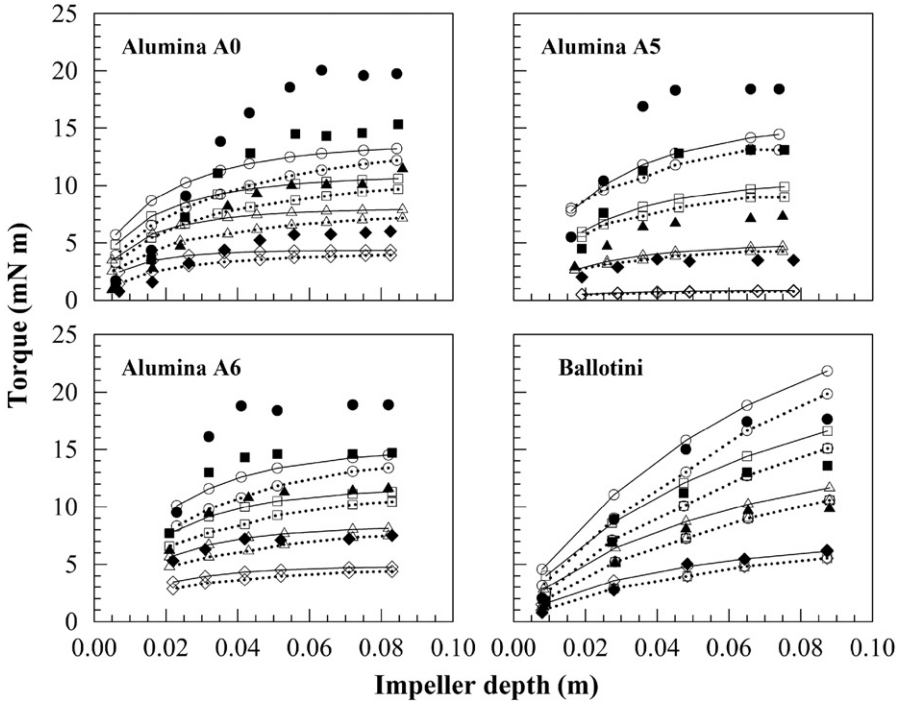

Fig. 6. Comparison between experiments and estimated torques values T vs. impeller depth z^* for different values of $\Delta P/\Delta P_c$ (symbols in Table 2). Filled symbols, experimental data. Hollow symbols and lines, predicted data: ————, model based on Janssen's approach; - - - -, model including Walker's improvements.

incorrect estimate of the wall friction angle, unrepresentative of the powder condition at the wall in the msFBR. This interpretation would be further confirmed by the better agreement for the ballotini sample. In this case, in fact, the lower value of the friction coefficient reduces its weight in the prediction of the torques.

5.2. Estimation of the flow properties with the msFBR

The ease of use of the msFBR may suggest its application the evaluation of the failure and flow properties of powders at low consolidation stress. Aeration, in fact, can be used to reduce the consolidation stress. In order to evaluate the powder flow

properties starting from torque measurements made at known depths and aeration levels, it was necessary to develop an inverse procedure able to estimate the effective angle of internal friction and the angle of wall friction.

To this purpose, the effective angle of internal friction was assumed as a constant parameter, to be determined, for each aeration rate tested. In fact, the upward gas flow exerts a drag force, opposed to gravity, which reduces the magnitude of the stresses inside the bed. Furthermore, the drag forces due to the gas flow increase as the aeration level increases and correspondingly increases the stress state reduction. Since aeration does not affect the rheology of powders (Klein et al., 2003; Johanson and Barletta, 2004; Barletta et al., 2007), it is reasonable to associate at each aeration rate, defined by the ratio $\Delta P/\Delta P_c$, a certain compaction condition of the powder in msFBR which, in turn, may affect the effective angle of internal friction.

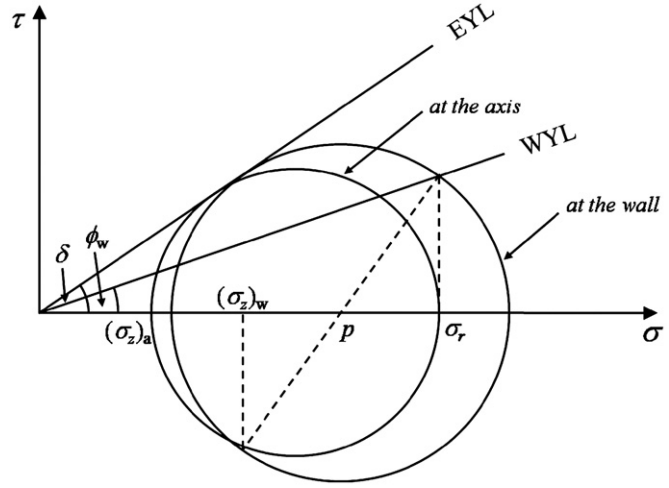

Fig. 7. Stress analysis according to Walker's improvements (Walters, 1973). At the container axis σ_r and $(\sigma_z)_a$ are principal stresses. σ_r is constant in the cross section and at the wall it is the normal stress that defines the point on the wall yield locus (WYL) representative of the wall stress. This point and the Mohr–Coulomb condition of tangency of the effective yield locus (EYL) define the Mohr's circle representative of the material stress state at the wall.

According to these hypotheses, constant values of δ and K were assumed for every aeration level and Eqs. (1) and (12) were solved analytically. This allowed to evaluate the stress distribution along the depth of the bed according to the Janssen approach (Bruni et al., 2007a):

$$\sigma_z(z^*) = \frac{(\rho_b g - (dP/dz))D}{4\mu_w K}\left[1-\exp\left(-\frac{4\mu_w K}{D}z^*\right)\right]$$

following Janssen's approach (22)

or according to the Walker improvements:

$$\overline{\sigma}_z(z^*) = \frac{(\rho_b g - (dP/dz))D}{4\mu_w K_W D}\left[1-\exp\left(-\frac{4\mu_w K_W \mathcal{D}}{D}z^*\right)\right]$$

including Walker's improvements (23)

where μ_w is the wall friction coefficient ($\mu_w = \tan\phi_w$).

Using Eqs. (22) and (23) in Eqs. (9), (10), (20) and (21), finite solutions for integrals (6) and (7) can be obtained to calculate torque values for the two models. Applying a regression procedure between each model and the experiments, it was possible to estimate with each of the two model the angle of wall friction ϕ_W, for each experimental material, and the effective angle of internal friction δ, for each material and aeration rate. The model results obtained with this procedure are given in Fig. 8, which shows the good level of approximation between model and experiments if both the value of δ and of ϕ_w are left free to change.

Corresponding values of δ estimated by the two models reported in Fig. 3 and can be compared with those measured with the annular shear cell. For each aeration level, the consolidation level was assumed corresponding to the major principal stress acting at the characteristic depth z_c of the stress state,

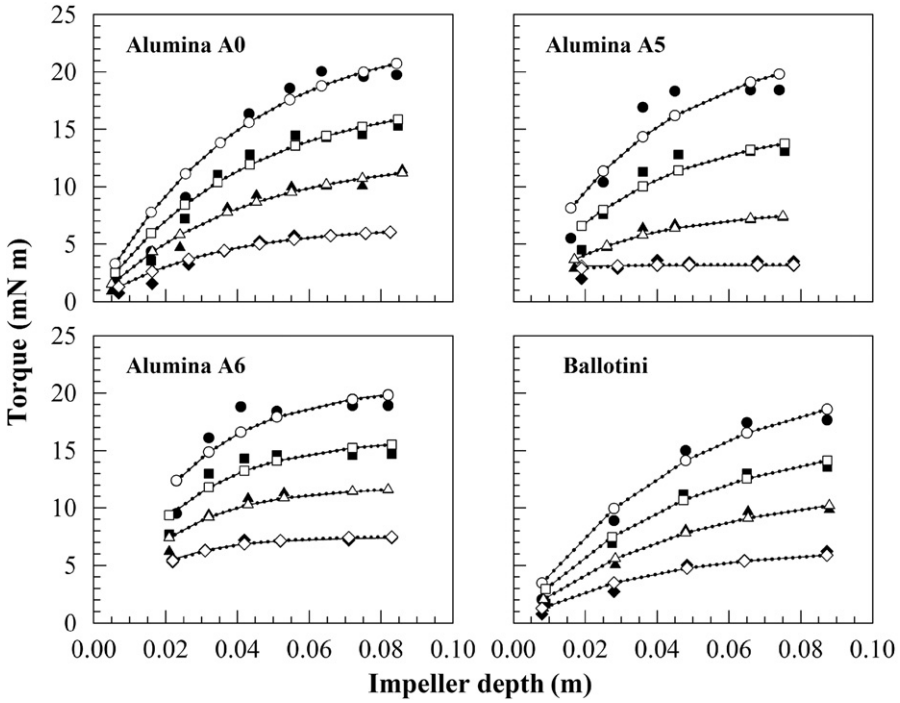

Fig. 8. Comparison between experiments and estimated torques values T vs. impeller depth z^* for different values of $\Delta P/\Delta P_c$ (symbols in Table 2). Filled symbols, experimental data. Hollow symbols and lines, regression of model when δ and of ϕ_w are left free to change: ————, model based on Janssen's approach; - - - -, model including Walker's improvements.

which governs the rate of approach to the asymptotic values of torques. Considering Eqs. (22) and (23), it is defined as

$$z_c = \frac{D}{4\mu_w K} \quad \text{according to Janssen} \tag{24}$$

$$z_c = \frac{D}{4\mu_w \mathcal{D} K_w} \quad \text{including to Walker's improvements} \tag{25}$$

Fig. 3 reveals a good match between experimental and estimated data, in particular for Alumina A0 and Ballotini, reporting significant changes only for Alumina A5 and A6 within the low consolidation stress range.

The estimated values of the angle of wall friction ϕ_W are reported in the last two columns of Table 1, countersigned by ([a]), when predicted by the model considering only the Janssen assumptions (Bruni et al., 2007a), and by ([b]), when calculated including the Walker improvements. Comparison in Table 1 of the values of ϕ_w measured with a Jenike tester with those obtained from the msFBR does not show the same consistency as the angle δ. In particular it is apparent that the msFBR technique tends to underestimate this data for alumina samples and to overestimate it for ballotini powder. It has to be recalled, however, that the measurement conditions of the wall friction angle in shear testers can differs significantly from the real process operating conditions on the powder and that it was not possible to evaluate the wall shear stress on exactly the same material of the msFBR walls. For this reason, values measured with the Jenike shear tester, could not be representative of the same conditions of the bulk solid at the msFBR wall. Furthermore, for glass ballotini, visual observations during wall friction measurement revealed particle rolling, which may not occur at the msFBR wall.

6. Conclusions

Two mathematical models, based on the Janssen approach to evaluate stresses in powder containers, allowed to relate the torque measurements carried out in a mechanically stirred Fluidized Bed Rheometer (msFBR) below the minimum for fluidization to the flow properties of the powder used and measured with standardized powder flow tester. The more accurate analysis performed by Walker (1966) and Walters (1973) does not introduce significant improvements in the evaluation of the stress distribution and in the prediction of the torque in the msFBR. Both models suggest that the hypothesis of a passive state of stresses in the material better predicts the torque profiles than the active state of stress, for all the powders and aeration rates tested.

A procedure for the inverse application of the model was developed and applied to estimate the powder flow properties starting from msFBR data. The results of the application of this procedure are good in terms of the effective angle of powder internal friction. Discrepancy with the wall friction angle suggest further studies, however the use of this apparatus and this procedure to evaluate powder flow properties is promising for the ability of the system to explore powder flow at very low consolidation states.

Nomenclature

A	msFBR cross-section area (m^2)
c	parameter in Eqs. (16) and (17) (dimensionless)
d	impeller size and diameter of the shearing cylinder around the impeller (m)
D	msFBR diameter (m)
$\mathcal{D}$	Walker's distribution factor (dimensionless)
d_p	mean particle diameter (m)
EYL	effective yield locus
F_{25}	size fraction < 25 μm (wt%)
F_{45}	size fraction < 45 μm (wt%)
g	acceleration due to gravity ($m\,s^{-2}$)
h	impeller height and height of the shearing cylinder around the impeller (m)
K	ratio between the radial and the axial normal stress (dimensionless)
K_W	ratio between the radial and the axial normal stress at the wall (dimensionless)
M	mass of powder in the bed (kg)
p	center of the Mohr circle (Fig. 7)
P	gas pressure (Pa)
r	radial coordinate in the msFBR (m)
T	torque (N m)
T_{down}	torque acting on the lower surface of the shearing cylinder (N m)
$T_{lateral}$	torque acting on the lateral surface of the shearing cylinder (N m)
T_{up}	torque acting on the upper surface of the shearing cylinder (N m)
WYL	wall yield locus
z	depth in the msFBR (m)
z_c	characteristic depth of the stress state (m)
z^*	impeller depth (m)

Greek letters

$\dot{\gamma}$	shear rate (s^{-1})
$\dot{\gamma}^*$	dimensionless shear rate (dimensionless)
δ	effective angle of internal friction (deg.)
ΔP	pressure drop across the bed (Pa)
ΔP_c	calculated pressure drop when full support is achieved (Pa)
θ	angular coordinate in the msFBR (deg.)
κ	active/passive state parameter (dimensionless)
μ_w	wall friction coefficient (dimensionless)
ρ_b	bulk density ($kg\,m^{-3}$)
ρ_p	particle density ($kg\,m^{-3}$)
σ	normal stress (Pa)
σ_1	major principal stress (Pa)
σ_r	normal stress in the radial direction (Pa)
$(\sigma_r)_w$	normal stress at the wall in the radial direction (Pa)
σ_z	normal stress in the z direction (Pa)
$(\sigma_z)_a$	normal stress at the axis of the msFBR in the z direction (Pa)
$(\sigma_z)_w$	normal stress at the wall in the z direction (Pa)
$\overline{\sigma}_z$	mean normal stress in the z direction on the cross section of the msFBR (Pa)
τ	shear stress (Pa)
$\tau_{r\theta}$	horizontal shear stress on the lateral surfaces of the shearing cylinder (Pa)
τ_w	wall shear stress (Pa)
$\tau_{z\theta}$	tangential shear stress on the horizontal surfaces of the shearing cylinder (Pa)
ϕ_w	angle of wall friction (deg.)
ω	parameter in Eqs. (14) and (15) (deg.)

Acknowledgments

The authors are indebted to the work of Dr. Giovanna Bruni from whose doctoral work the present paper originated and found its motivation.

References

Barletta, D., Donsì, G., Ferrari, G., Poletto, M., 2007. A rotational tester for the characterization of aerated shear flow of powders. Part. Part. Syst. Charact. 24, 259–270.

Bruni, G., Barletta, D., Poletto, M., Lettieri, P., 2007a. A rheological model for the flowability of aerated fine powders. Chem. Eng. Sci. 62, 397–407.

Bruni, G., Colafigli, A., Lettieri, P., Elson, T., 2005. Torque measurements in aerated powders using a mechanically stirred fluidised bed rheometer (msFBR). Chem. Eng. Res. Des. 83, 1311–1318.

Bruni, G., Lettieri, P., Newton, D., Barletta, D., 2007b. An investigation of the effect of the interparticle forces on the fluidization behaviour of fine powders linked with rheological studies. Chem. Eng. Sci. 62, 387–396.

Castellanos, A., Quintanilla, M.A.S., Valverde, J.M., Soria-Hoyo, C., 2007. Novel instrument to characterize dry granular materials at low consolidations. Rev. Sci. Instrum. 78, 073901.

Castellanos, A., Valverde, J.M., Quintanilla, M.A.S., 2004. The Sevilla Powder Tester: a tool for characterizing the physical properties of fine cohesive powders at very small consolidations. KONA 22, 66–81.

Daniher, D.I., Zhu, J., 2008. Dry powder platform for pulmonary drug delivery. Particuology 6, 225–238.

EN 1991-4, 2006. Eurocode 1 – actions on structures – Part 4: silos and tanks.

Harnby, N., 2000. An engineering view of pharmaceutical powder mixing. Pharm. Sci. Technol. Today 3, 303–309.

Janssen, H.A., 1895. Versuche über Getreidedruck in Silozellen. Z. Ver. Dt. Ing. 39, 1045–1049.

Johanson, K., Barletta, D., 2004. The influence of air counter-flow through powder materials as a means of reducing cohesive flow problems. Part. Part. Syst. Charact. 21, 316–325.

Kheiripour Langroudi, M., Turek, S., Ouazzi, A., Tardos, G.I., 2010. An investigation of frictional and collisional powder flows using a unified constitutive equation. Powder Technol. 197, 91–101.

Klein, J., Höhne, D., Husemann, K., 2003. The influence of air permeation on the flow properties of bulk solids. Chem. Eng. Technol. 26, 139–146.

Kwade, A., Schulze, D., Schwedes, J., 1994. Determination of the stress ratio in uniaxial compression tests. Part 2. Powder Handling Process. 6, 199–203.

Nedderman, R.M., 1992. Statics and Kinematics of Granular Materials. Cambridge University Press, Cambridge.

Schulze, D., Wittmaier, A., 2003. Flow properties of highly dispersed powders at very small consolidation stresses. Chem. Eng. Technol. 26, 133–137.

Schwedes, J., 2003. Review on testers for measuring flow properties of bulk solids. Granular Matter 5, 1–43.

Standard Shear Testing Technique for Particulate Solids Using the Jenike Shear Cell, 1989. The Institution of Chemical Engineers. Rugby, UK.

Suri, A., Horio, M., 2009. A novel cartridge type powder feeder. Powder Technol. 189, 497–507.

Tardos, G.I., Khan, M.I., Schaeffer, D.G., 1998. Forces on a slowly rotating, rough cylinder in a Couette device containing a dry, frictional powder. Phys. Fluids 10, 335–341.

Tardos, G.I., McNamara, S., Talu, I., 2003. Slow and intermediate flow of a frictional bulk powder in the Couette geometry. Powder Technol. 131, 23–39.

Walker, D.M., 1966. An approximate theory for pressures and arching in hoppers. Chem. Eng. Sci. 21, 975–997.

Walters, J.K., 1973. A theoretical analysis of stresses in silos with vertical walls. Chem. Eng. Sci. 28, 13–21.